Nanoscale

PAPER

Cite this: *Nanoscale*, 2016, **8**, 889

Field-directed assembly of nanowires: identifying directors, disruptors and indices to maximize the device yield†

Mahshid Sam, Nima Moghimian and Rustom B. Bhiladvala*

Received 30th September 2015,
Accepted 1st November 2015

DOI: 10.1039/c5nr06763d

www.rsc.org/nanoscale

Individually-addressable nano-electro-mechanical (NEMS) devices have been used to demonstrate sensitive mass detection to the single-proton level, as well as neutral-particle mass spectrometry. The cost of individually securing or patterning such devices is proportional to their number or the chip area covered. This limits statistical support for new research, as well as paths to the commercial availability of extraordinarily sensitive instruments. Field-directed assembly of synthesized nanowires addresses this problem and shows potential for low-cost, large-area coverage with NEMS devices. For positive dielectrophoresis (pDEP) as the main assembly director, the space of field, geometric and material parameters is large, with combinations that can serve either as directors or disruptors for directed assembly. We seek parameter values to obtain the best yield, by introducing a rational framework to reduce trial-and-error. We show that sorting the disruptors by severity and eliminating those weakly coupled to the director, allows reduction of the parameter space. The remaining disruptors are then represented compactly by dimensionless parameters. In the example protocol chosen, a single dimensionless parameter, the yield index, allows minimization of disruptors by the choice of frequency. Following this, the voltage may be selected to maximize the yield. Using this framework, we obtained 94% pre-clamped and 88% post-clamped yield over 57000 nanowire sites. Organizing the parameter space using a director–disruptor framework, with economy introduced by non-dimensional parameters, provides a path to controllably decrease the effort and cost of manufacturing nanoscale devices. This should help in the commercialization of individually addressable nanodevices.

1 Introduction

Remarkable capabilities of single-proton mass detection,[1] neutral particle mass spectrometry[2] and earlier, the detection of nucleic acid sequences[3] have been demonstrated using individually addressable nano-electro-mechanical (NEMS) devices, but only for a small number of clamped nanowires (NWs) or nanobeams. Large-area coverage with individually-addressable NW devices will significantly reduce the experimental research time for future landmark demonstrations. If done at low cost, it will also enable stronger statistical support for measurements needed to understand the mechanical[4–7] and electrical[4,8,9] behavior of NWs, and most significantly, ease the development of instruments for commercial applications, such as screening for early detection of disease through molecular diagnosis.[10] A recent review[11] provides several examples of promising NW device applications.

Directed assembly provides a path towards nanomanufacturing systems to achieve large-area coverage at low-cost. For nanofabrication, the term "directed assembly" describes a family of methods[12–16] which use micro-patterned structures for spatial and temporal control of fields, to direct the synthesized nanoscale elements to predetermined locations. The patterned structures enable NW position control and could involve one of several fields such as hydrodynamic, electric, magnetic, temperature -or their combinations. Such field-directed assembly combines elements of top-down microfabrication and bottom-up nanostructure synthesis, enabling fabrication of nanoscale devices in large arrays. It retains the advantages of using low-cost nanostructure assembly (compared to electron-beam lithographic patterning) offered by self-assembly,[16,17] but also provides greatly improved position control, and a route to individual device addressability.

In contrast with established macroscale manufacturing processes, research laboratory nanofabrication protocols,

Department of Mechanical Engineering, Center for Advanced Materials and Related Technologies (CAMTEC) and Integrated Energy Systems at the University of Victoria (IESVic), University of Victoria, Victoria, BC, Canada. E-mail: rustomb@uvic.ca

†Electronic supplementary information (ESI) available: This section includes micrographs of high yield pre- and post-clamped nanowires. See DOI: 10.1039/C5NR06763D

including field-directed assembly, often require minor modifications, to be reproducible by a new user or in a new facility. Missing information arising from unknown methods or prohibitive cost of adequate metrology at device scale is one cause of these minor deviations in repeatability of protocols. In addition, there is an imperfect understanding of possible coupling between several physical effects, as discussed in the example protocol chosen for this paper. As a result, a user who decides to change a single step, material or experimental parameter value within a protocol may often have to change several others. In the absence of a framework to guide the choice of experimental parameter values, considerable effort is required in a trial-and-error approach to obtain the best yield from NW assembly. To strongly reduce such effort, we propose a framework, based on identifying forces, which serve either as directors or disruptors, with competing effects on the yield in directed assembly. The framework provides a rational guide to parameter value selection.

Dielectrophoretic (DEP) force has been reported by a few research laboratories[9,12–15,18–21] worldwide, as a director in field-directed NW assembly. Examples of directors and disruptors are forces that arise from negative or positive DEP,[21] Brownian motion,[22,23] electroosmotic forces[14,20] or electrode polarization effects.[14,18] Here we use a sequence of basic steps from a known DEP protocol, reported in the work of Li *et al.*,[15] to help illustrate the utility of the framework. Starting with an established basis is also necessary to examine whether any improvements in yield accrue from the use of the framework.

While the parameter values are chosen using the framework developed later in this paper, here we briefly outline the basic steps utilized, as shown in Fig. 1(a)–(d). We used rhodium (Rh) NWs that have desirable mechanical properties for resonant mass sensing as they retain a high quality factor (*Q*-factor) from high vacuum to near atmospheric pressure.[15] Photolithography was first used to create electrically conductive pad pairs with different gap widths of 6, 8 and 10 μm, which define the locations to which NWs will be directed. A photoresist layer was spun to cover the electrodes and prevent an electrical short circuit that would result from NWs bridging the electrode pads. Wells (shown in Fig. 1(a)) were then patterned in the photoresist, between each electrode pair, followed by application of the electric field to direct NWs from a suspension into the wells (Fig. 1(b)). The photoresist was removed from one of the electrode pairs and a clamp material was electrodeposited to fix one end of the NWs (Fig. 1(c)). Finally, the NWs were suspended (Fig. 1(d)) by removing the remaining photoresist from the substrate and using critical point drying. Experimental details may be found in section 4 at the end of this paper.

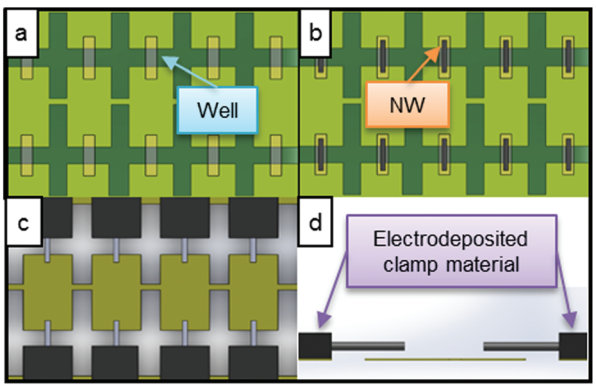

Fig. 1 Schematics of positioning and clamping of single NWs on gold electrodes: (a) patterning electrode pairs with wells in between, to locate and trap NWs, (b) positioning single NWs inside wells using DEP, (c) electrodeposition of the clamp material after photoresist removal from the electrode surface, (d) side view of clamped NWs after removing the remaining photoresist.

The word "yield" in the literature on directed assembly has been used to refer to different things. Most devices made from suspended NWs need one or both ends to be clamped after the directed assembly process is complete. Though clamping processes typically do reduce the yield, the word "yield" has been used to report the yield from assembly alone,[12,19] while other reports[15] use the word to mean the yield of functional devices after both assembly and clamping. It is misleading to compare numbers for the yield between these two groups of references. To avoid confusion, we suggest the use of two categories of NW yield: pre-clamped yield, which is the percentage of available sites with correctly positioned single NWs; and post-clamped yield, referring to the percentage of sites with functional, clamped NWs.

2 Framework development

This study is focused on developing a framework for field-directed assembly of NWs. A DEP protocol with positive dielectrophoresis (pDEP) as the main director is used here to show the framework methodology in classifying and evaluating the directors and disruptors. We separate disruptors into two groups: {1} disruptors weakly coupled to the main director, pDEP, that either depend on the electrode design or need less quantification to be eliminated and {2} disruptors that are strongly coupled through the choice of parameter values to the main director. In this section, we first evaluate the weakly-coupled disruptors (disruptive torque, capillary force from the drying front, inappropriate NW concentration, Brownian motion and electrothermal force) followed by the strongly-coupled ones (negative DEP (nDEP), electroosmotic force and electrode polarization). In this evaluation, the results of analysis and computation can provide useful guidance, even if somewhat rough. This step is followed by the definition of a dimensionless parameter, which compactly represents the competition between the director and the remaining disruptors. This helps to guide parameter value selection for the best device yield, with reduced trial-and-error. In the example chosen in this study, the final control of the device yield was realized only by tuning the director, with negligible hindrance from the disruptors.

2.1 Weakly-coupled disruptors

2.1.1 Disruptive torque. DEP torque, here the primary director for NW alignment, can become a disruptor when NWs are much longer than the width of the gap between electrodes, in each electrode pair. For low values of the ratio (λ) of the electrode gap width to the NW length, the induced dipoles can lie beyond the two electrode edges, rather than in between them, with a torque that rotates the NWs in an opposite sense to that required for alignment (disruptive or "negative" torque). Some guidance is provided by the computational results of Liu *et al.*,[22] which show that it is possible to avoid disruptive torque if $\lambda > 0.4$, that is, when NW length is smaller than 2.5 times the gap width.

NWs of length smaller than the gap width ($\lambda > 1$) clearly cannot have both ends clamped, and may produce one-end clamped devices which are outside the intended functional range, even if they are properly aligned. To avoid this, we restrict our choices to the range ($0.4 < \lambda < 1$).

2.1.2 Capillary force. The spreading of a drop of the NW suspension during assembly carries NWs beyond the target assembly region and often leads to undesirable spillover on adjacent dies. Vigorous NW motion was observed during such drop spreading, acting as a disruptor. A further disruptive role of the capillary force was seen at drying fronts, that pull away the NWs which are partially protruding from the wells.

To reduce these disruptive effects, we introduced a cylindrical dam (Fig. 2) with 1 cm diameter and 0.5 cm height, which confined the NW suspension to the area of one die with 9500 wells. This eliminates spreading and flow disruption and allows sufficient time for DEP to secure both NW ends within the wells.

2.1.3 Inappropriate nanowire concentration. Having too low a concentration will lead to unfilled sites. For any selected suspension volume, a concentration allowing at least one NW for each well (equivalent to 9.5×10^5 NW per mL) is clearly needed to avoid empty sites. However, too high a NW concentration can lead to the formation of chains, bundles, or multiple NWs assembled between electrode pairs, disrupting single-NW assembly and reducing the yield. Using the procedure in section 4, we determined by experiment that a concentration of 19×10^5 NW per mL (2 NWs for each well) was suitable, and it repeatedly allowed us to avoid problems associated with too high a concentration of NWs. Images of NW assembly with different NW concentrations are provided in Fig. S1.†

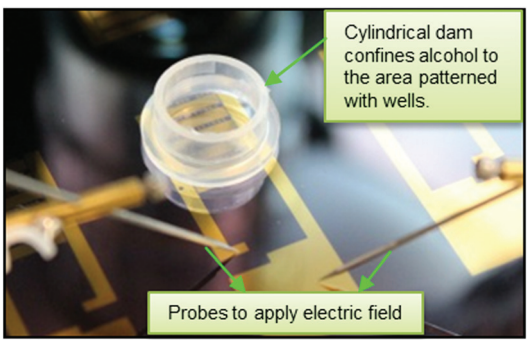

Fig. 2 A cylindrical dam reduces the effects of the drying-front capillary force as a disruptor and prevents the NW spillover to adjacent dies.

2.1.4 Brownian motion. In our experiments, random displacement of NWs due to Brownian motion was observed when no electric field was applied. However, when the electric field was applied, we observed that NW trapping within the wells began in about a second after the NW suspension was introduced.

In spite of our observation for this assembly process, we ask how significant a disruptor Brownian motion could be, and in what circumstances. Cumulative Brownian displacement could be disruptive if it is comparable to, or greater than the displacement due to the DEP force. It is less likely to be disruptive when very close to the electrode edges, where the field gradient and DEP force are the strongest, but has the scope to disrupt motion along the capture path at large distances from the electrode. The ratio of the root-mean-squared (rms) NW displacement induced by Brownian motion to DEP displacement has been estimated earlier[22,23] for spherical particles. We obtained results for cylindrical NWs, moving perpendicular to the NW axis, in low Reynolds number flow. For this case, the drag coefficient is given by[24]

$$\gamma = F_d/u = 4\pi\eta L/[\ln(2L/d) + 0.5] \quad (1)$$

Here L and d are the NW length and diameter respectively, the drag force is F_d, u is the velocity of the NW relative to the fluid and η is the dynamic viscosity of the fluid. With L = 10 μm, d = 0.25 μm and $\eta = 1.2 \times 10^{-3}$ Pa s for ethanol, the drag coefficient value is 3.09×10^{-8} kg s^{-1}. The reader is referred to the steps in the Appendix of this manuscript, for derivation of the ratio of Brownian to DEP displacement, in the elapsed time t, which yields,

$$\Delta X_{Br}/\Delta X_{DEP} = \sqrt{(2k_BT)/(u^2\gamma t)} = \sqrt{(2K_BT\gamma)/(F^2 t)} \quad (2)$$

Here F is the DEP force, equal to the drag force on the NW at terminal velocity, k_B is the Boltzmann's constant and the absolute temperature T = 293 K. The ratio is inversely proportional to the NW velocity, and decreases with the elapsed time as $t^{-1/2}$. There is no known way of measuring the forces, or velocities normal to the observation plane, for individual NWs during this assembly process, and we expect that both will depend on the NW height above electrodes. However, we may use eqn (2) to examine the role of Brownian motion from an order of the magnitude estimate. The fluid depth in the dam is ~100 μm. An assembly time ~1 s, for a distant NW in the vicinity of the fluid–air interface, yields an estimate for the maximum NW velocity of ~100 μm s^{-1}, for which the value of $\Delta X_{Br}/\Delta X_{DEP}$ is calculated to be 0.005. For a more reasonable starting NW distance of ~10 μm, the velocity would be ~10 μm s^{-1}, and this ratio would be 0.05. The NWs at the starting distances ~1 μm or lower would be in the highest field gradient region and close to be captured within the wells. In accord with our experi-

mental observations, this rough estimation process confirms that Brownian motion is not a significant disruptor.

However, the value of this rough scaling analysis is that it shows that Brownian motion could be a significant disruptor for slow-moving NWs, low DEP force and for liquids at low temperatures or with high viscosity.

2.1.5 Electrothermal force. Electrothermal force is another disruptor for DEP-assisted positioning of NWs. The current due to the applied electric field causes local heat generation in the solution. The resulting temperature variation, if significant, would lead to conductivity and permittivity gradients in the fluid. Therefore, the force imposed on the medium by the electric field can vary in different parts of the fluid and induce fluid flow, named electrothermal flow, which interacts with NW positioning. The fluid temperature change is given by:[22,23]

$$\Delta T \approx \frac{\sigma_m {V_{rms}}^2}{2K} \quad (3)$$

where K and σ_m are thermal and electrical conductivities of the fluid medium respectively (K = 0.171 W m^{-1} K^{-1} and σ_m is 2.19 × 10^{-5} S m^{-1} for ethanol[25]). The maximum applied voltage in this work, V_{rms} = 7 V yields a temperature rise of about 10^{-3} °C. For this small temperature change, the effect on the permittivity and conductivity is negligible, hence electrothermal fluid flow is not considered as a disruptor in this work.

In this section, we have used the results of analysis and computation as a rough guide to (a) find which potential disruptors are negligible (here, Brownian motion and electrothermal force) and (b) impose constraints on physical parameters (such as the ratio of the electrode gap width to the NW length) to make disruptors negligible. We also used experiments to eliminate some potential disruptors (capillary force and inappropriate NW concentration). Enforcing these constraints reduces the dimension of the parameter space. If there is a resurgence of disruptors when modifications are made to the established parameter values for a given protocol, these constraints provide a path for correction. This greatly reduces the time spent compared to a trial-and-error approach with little intuition.

2.2 Strongly-coupled disruptors

2.2.1 Negative DEP. The time averaged DEP force is given by:[21,26]

$$F_{DEP} = \frac{\pi r^2 l}{6} \varepsilon_m \mathrm{Re}[F_{CM}] \cdot \nabla \left({E_l}^2\right) \quad (4)$$

with

$$F_{CM} = \frac{\varepsilon_p^* - \varepsilon_m^*}{\varepsilon_m^*} \quad (5)$$

where l and r are the length and radius of a NW, ε_m is the permittivity of the medium and E_l is the electric field. Re[F_{CM}], the real part of the Clausius–Mossotti factor, is positive over a range of frequencies for conductive NWs suspended in alcohol and becomes negative at sufficiently high frequencies.[20,26]

ε_p^* and ε_m^* are the complex permittivities of the NWs and medium respectively, defined as $\varepsilon^* = \varepsilon - j\left(\frac{\sigma}{\omega}\right)$ where ω is the angular frequency of the applied electric field. The sign of Re[F_{CM}] dictates the sign of F_{DEP}. NWs are attracted to or repelled from the wells when F_{DEP} is positive or negative, respectively. Here, we eliminate nDEP simply by choosing frequencies below 10^{10} Hz (Fig. 3(a)), ensuring that DEP remains solely a director. Later in this paper, we will see that other constraints on the frequency compel us to use frequencies well below 10^{10} Hz.

2.2.2 Electroosmotic velocity. Among the electrohydrodynamic (EHD) effects, a strong potential disruptor in this work is electroosmotic flow, which can interfere with NW positioning by creating a vortical flow, as shown in Fig. 3(b). This flow is driven by the electroosmotic force $F = qE_t$, where E_t is the tangential component of the electric field and q is the surface charge density of the electrical double layer. Green *et al.*[27] and Castellanos *et al.*[23] showed that the electroosmotic fluid velocity strongly depends on the applied frequency. In addition, eqn (5), plotted in Fig. 3(a), shows that Re[F_{CM}] and as a result F_{DEP}, also depends on the frequency. We show below, that a careful choice of frequency can be used to overcome the disruptive effect of the electroosmotic flow.

The electroosmotic velocity, ν, can be calculated using[27]

$$\nu = \frac{\varepsilon_m {V_{rms}}^2}{4x\eta} \times \frac{\Omega^2}{(1+\Omega^2)^2} = \frac{\varepsilon_m {V_{rms}}^2}{4x\eta} f(\Omega) \quad (6)$$

knowing the rms-value of the applied voltage (V_{rms}), dynamic viscosity of the electrolyte (η) and characteristic length x (half the gap width between electrodes), and with Ω, the dimensionless frequency, defined as:

$$\Omega = \frac{\pi}{2} x\kappa\omega\left(\frac{\varepsilon_m}{\sigma_m}\right) \quad (7)$$

where κ is the reciprocal Debye length of the double layer. For liquids with a low dielectric constant, such as ethanol, κ^{-1} is ~0.5 μm.[28] The electroosmotic velocity is plotted in Fig. 3(c) for ethanol with ε_m = 2.3 × 10^{-10} F m^{-1} and σ_m = 2.19 × 10^{-5} S m^{-1}, at V_{rms} = 7 V and characteristic length of x = 5 μm. It shows a frequency peak at ~10^3 Hz, which is termed as the EO-characteristic frequency. At low frequencies, here below ~10^2 Hz, the voltage drop across the double layer is high, making E_t small, with the resulting electroosmotic force $F = qE_t$ being too small to create the electroosmotic flow. At high frequencies, here above ~4 × 10^4 Hz, we do not see the electroosmotic flow, but for a different reason. At this high frequency the double layer does not have sufficient time to form,[23,27] and the electroosmotic force is small because q is small. The calculation above provides guidance for selecting the frequency to minimize the electroosmotic flow. In addition, to enable the use of a normalized electroosmotic velocity, (ν/ν_{max}), as a dimensionless measure of the strength of this disruptor, we note, from eqn (6) that the maximum value of $f(\Omega)$ occurs at Ω = 1, yielding $\nu_{max} = (\varepsilon_m {V_{rms}}^2)/(16x\eta)$. This parameter, ν_{max}, is used in section 2.4.

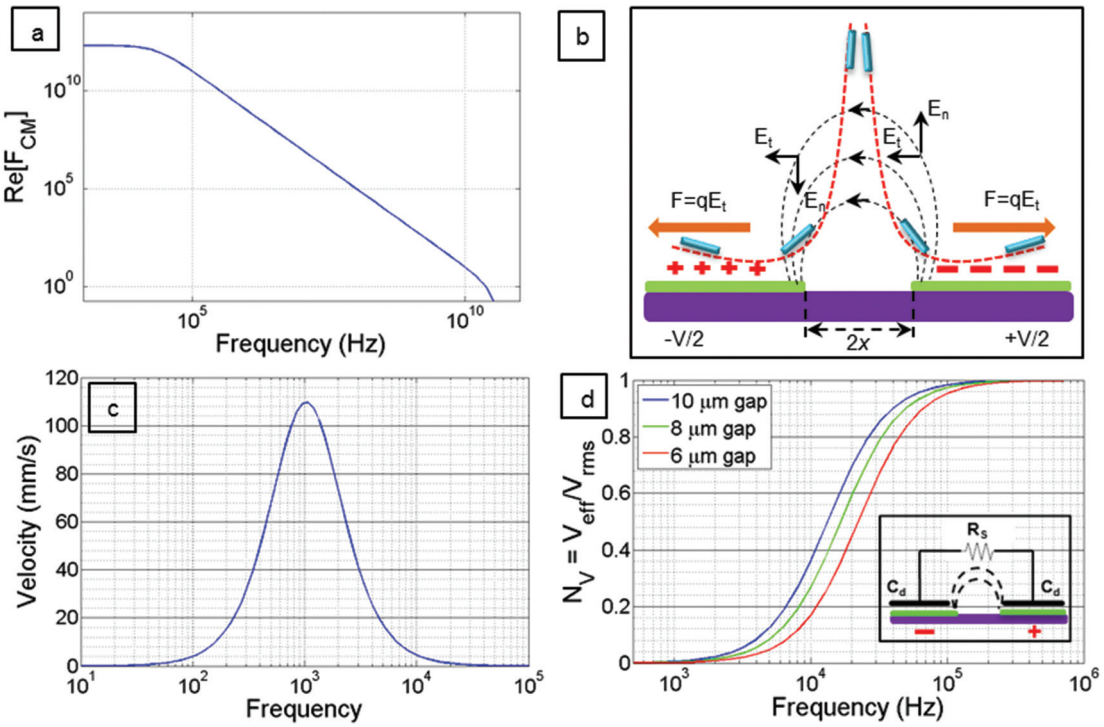

Fig. 3 Frequency changes affect the competing director and disruptor forces by altering (a) the magnitude of the DEP director as a result of the change in the magnitude of Re[F_{CM}]; (b) the electroosmotic force (F), a disruptor that drags NWs away from the assembly-electrode gap and (c) the electroosmotic velocity of disruptor fluid vortices. (d) The ratio of the effective voltage to the applied voltage for different gap sizes changes with frequency due to electrode polarization (a disruptor), modeled as an RC circuit (inset).

2.2.3 Electrode polarization. The presence of an electrical double layer gives rise to another disruptor, electrode polarization. Electrode polarization causes a voltage drop adjacent to the electrode, and as a result, the effective voltage (V_{eff}) that provides the field strength for NW positioning, becomes less than the applied voltage (V_{rms}). The electrical conduction path, shown in Fig. 3(d) (inset) consists of electrolyte resistance R_s for conduction through the suspending medium with two capacitive impedances (C_{eq}) in series, associated with the electrical double layers and photoresist at each of the two electrodes. The total impedance Z_T is defined[29,30] by:

$$Z_T = R_s\left[1 + \frac{2}{j\omega C_{eq} R_s}\right] \tag{8}$$

Here $C_{eq} = [C_d C_{PR}/(C_d + C_{PR})]$, where C_d and C_{PR} are the capacitances of the electrical double layer and the photoresist layer over the electrode, respectively. For the electrodes of surface area S, with the photoresist thickness of t and κ^{-1} as a measure of the double-layer thickness, $C_d = \varepsilon\kappa S$ and $C_{PR} = \varepsilon t^{-1} S$. R_s is calculated by approximating the conduction path as having length equal to the gap size ($2x$) and a cross-section defined by the electrode width and a measure of the double-layer thickness, κ^{-1}.

The ratio (V_{eff}/V_{rms}), the normalized effective voltage for DEP, may be defined, as seen in the inset of Fig. 3(d), by:

$$N_V = \frac{V_{eff}}{V_{rms}} = \left|\frac{1}{1 + \frac{2}{j\omega R_s C_{eq}}}\right| = \frac{1}{\sqrt{1 + \left(\frac{2}{\omega R_s C_{eq}}\right)^2}} \tag{9}$$

The minimum normalized effective voltage for DEP ($N_V = 0$) occurs when the electrode polarization disruptor effect is maximum and *vice versa*. Therefore, normalized electrode polarization is defined as:

$$N_{EP} = 1 - N_V \tag{10}$$

Fig. 3(d) shows that at frequencies less than 10^5 Hz only a fraction of the applied voltage is available for NW positioning and below 10^3 Hz, N_V goes to zero as the value of N_{EP} approaches 1. As seen from a curve for any single value of the gap size in Fig. 3(d), we may maximize the fraction of the applied voltage available for DEP to $N_V = 1$ by increasing the frequency. Our choice of the electrode gap size is determined by the NW length and the constraint to avoid disruptive torque. How does this choice affect the strength of electrode polarization as a disruptor?

The effect of varying the electrode gap size is seen in the curves in Fig. 3(d), which shows that electrode polarization vanishes at higher frequencies for a smaller electrode gap size ($2x$). This effect can be explained by the effect of relaxation times defined by Bazant *et al.*[31] as $\tau_c = 2x\kappa^{-1}/D$ where D is the ion diffusivity. Larger gap widths ($2x$) require a longer charging time τ_c, and a lower frequency must be used to achieve the same double-layer thickness. As seen in Fig. 3(d), if the same frequency is used for larger gaps, the effective voltage available for the DEP field is increased, reflecting the reduced double-layer thickness.

2.3 Experimental observation: effect of strongly-coupled disruptors on assembly yield

In the last section, we have shown that frequencies higher than 10^5 Hz would be required to eliminate both electro-osmotic flow and electrode polarization disruptors. To see the effect of these disruptors on the yield, the pre-clamped yield was measured at two frequencies: {1} 10^4 Hz, at which the theoretical results in Fig. 3(d) show that only ~16, 28 and 38% of the applied voltage is effective for NW assembly for the gap sizes of 6, 8 and 10 μm respectively, and {2} 10^5 Hz, where V_{eff} is almost equal to V_{rms}. If the theoretical results in Fig. 3(c) and (d) are accurate, pre-clamped assembly yield should show a significant increase at 10^5 Hz, compared to 10^4 Hz. The experimental results are shown in Table 1 and Fig. 4.

{1} After eliminating weakly-coupled disruptors by following the guidelines provided in section 2.1, NW assembly between electrodes with the gap sizes, $2x$, equal to 6, 8 and 10 μm, was observed at 10^4 Hz. Almost no assembly occurred at voltages less than 7 V (rms) at this frequency. Increasing the applied voltage to the maximum value available to us, 7 V (rms), 15 to 20% of the wells filled with NWs. For each gap size, V_{eff}/V_{rms} at 10^4 Hz (based on Fig. 3(d)) and the experimental yield of the pre-clamped NWs are shown in Table 1.

{2} The yield was then studied for a range of voltages between 0.7 and 7 V (rms) at 10^5 Hz as shown in Fig. 4. For each gap size, there is a threshold voltage below which NW assembly does not occur due to the small value of F_{DEP}. As seen in Fig. 4, NW assembly does not occur at voltages below 2, 1 and 0.7 V (rms) for 10, 8 and 6 μm gap sizes respectively. Increasing the applied voltage and resulting F_{DEP} increases the assembly yield. The maximum yield realizable occurs at the highest available voltage of 7 V (rms) at 10^5 Hz. For this condition, we used two dies of 9500 sites, for each gap size. The measured pre-clamped yield varied with the gap size. Several optical micrographs such as in Fig. 5, were used to determine the yield. The yields were 91% and 93% for the 10 μm gap, 94% and 95% for 8 μm and 94% and 96% for the 6 μm gap size, resulting in an averaged pre-clamped yield of 94%.

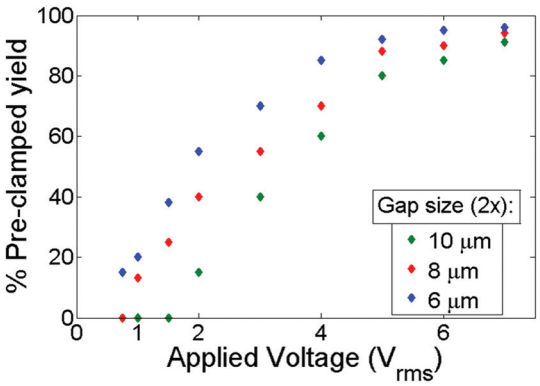

Fig. 4 Experimental results showing the effect of the applied voltage on the pre-clamped yield at 10^5 Hz for three different gap sizes ($2x$). Larger gap sizes have higher threshold voltages (2, 1 and less than 0.7 V (rms) respectively) for $2x$ = 10, 8 and 6 μm. Highest assembly yield occurs at 7 V (rms).

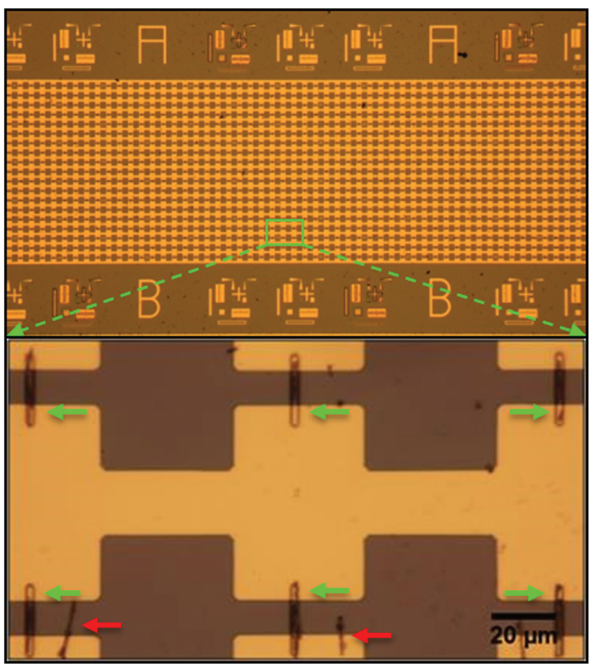

Fig. 5 Single NWs aligned in almost every well (green arrows) at 10^5 Hz and 7 V (rms). Red arrows show misaligned NWs.

Table 1 Pre-clamped experimental yield (Exp. yield) at 10^4 Hz and 7 V (rms). Theoretical V_{eff}/V_{rms} was calculated using Fig. 3(d)

Gap size (μm)	V_{eff}/V_{rms}	Exp. yield (%)
10	0.38	20
8	0.24	18
6	0.18	15

2.4 Director–disruptor competition

To separate the director-dominant region from the region of competition, seen in Fig. 6(a) and (b), we introduce a cut-off frequency, at which both the strong disruptors, normalized electroosmotic velocity (N_{EO}) and normalized electrode polar-

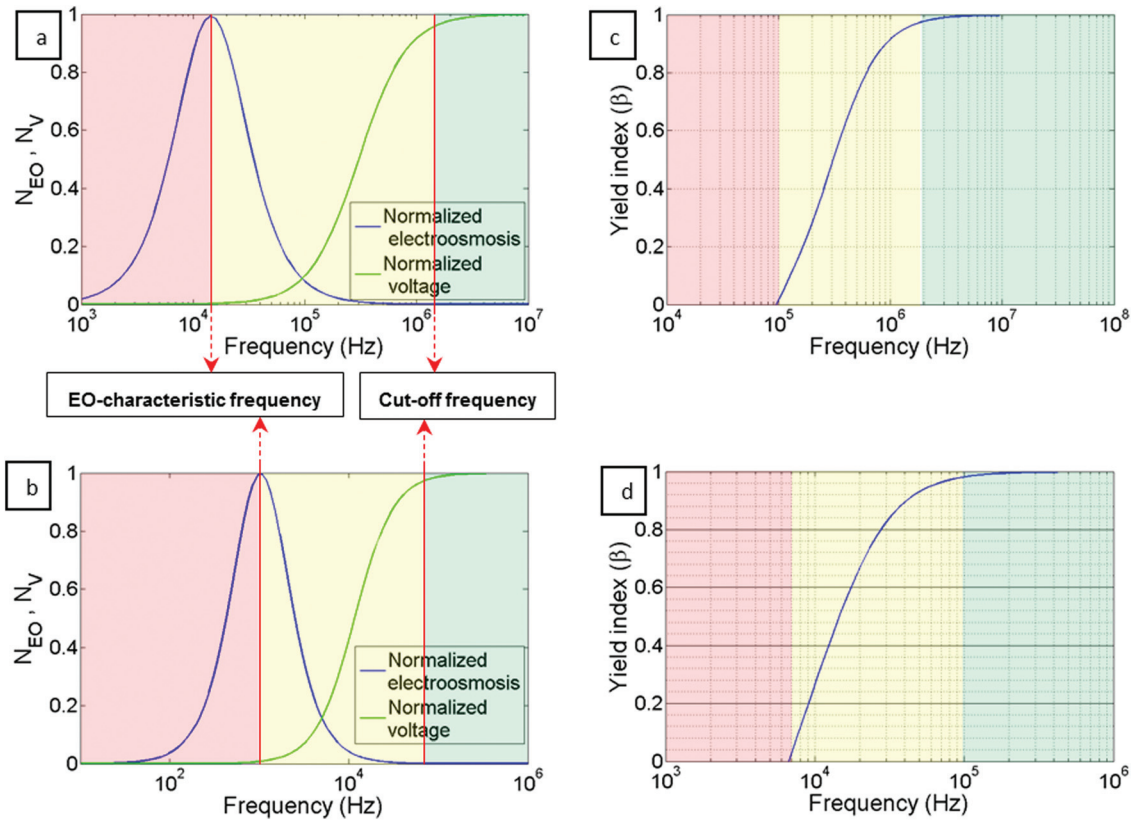

Fig. 6 Director-dominant (green), disruptor-dominant (pink) and competing region (yellow) for water (a) and ethanol (b) with electrical conductivities of 5.0×10^{-3} and 2.2×10^{-5} S m^{-1} respectively. The yield index for water (c) and ethanol (d) indicates that a higher frequency is required for the effect of disruptors to be negligible in water, compared to ethanol. For this comparison, electrode gap size was 10 μm and 1 μm photoresist layer was considered on the electrodes.

ization ($N_{EP} = 1 - N_V$) are each less than 5%. The normalized electroosmotic velocity N_{EO} is defined as:

$$N_{EO} = \frac{\nu}{\nu_{max}} = \frac{4\Omega^2}{(1+\Omega^2)^2} \quad (11)$$

where ν_{max} defined in section 2.2.2, is the maximum electroosmotic velocity at the EO-characteristic frequency. N_{EO} provides a non-dimensional measure of the strength of this disruptor.

The regions with frequencies higher than the cut-off frequency are the director-dominant regions. If the DEP force in this frequency range is large enough to direct NWs, it will face negligible competition from disruptors in this region. Fig. 6(b) shows that when ethanol is used as the medium, a large disruptor-free frequency range is available, beginning at ~10^5 Hz and extending to ~10^{10} Hz, the frequency for cross-over into the nDEP region.

The region with frequencies less than the EO-characteristic frequency (peak) is disruptor-dominant. Here high electrode polarization and the electroosmotic fluid flow overcome the directive effect of the DEP force and decrease the yield dramatically. At frequencies between the cut-off and EO-characteristic frequencies, as seen in the central region of Fig. 6(a) and (b), the directors and disruptors are competing. The cut-off and EO-characteristic frequencies vary as the medium changes, since both N_{EO} and N_V depend on the electrical properties of the medium. To investigate the effect of the suspension medium properties, we chose water and ethanol and plotted N_{EO} and N_V *vs.* frequency. Fig. 6(a) and (b) shows the three regions for water and ethanol respectively. The higher cut-off and EO-characteristic frequencies for water compared with ethanol are due to the higher conductivity of water.

The competing region is an important region to study as the competition between forces can decrease or increase the device yield. How can the effect of competition between the director and the dominant remaining disruptors on the device yield be approached quantitatively? As we have earlier (in section 2.1) removed the weakly-coupled disruptors, we now define a parameter, the yield index β, such that $\beta = 1$ if there is no reduction of DEP by disruptors and $\beta = 0$, if the disruptors are at their maximum value. β is defined as:

$$\beta = 1 - N_{EP} - N_{EO} \quad (12)$$

Using eqn (10), this can be rewritten as:

$$\beta = N_V - N_{EO} \quad (13)$$

Fig. 6(c) and (d) show how the region of competition and the resulting yield index change with respect to frequency in water and ethanol respectively. For our selected parameter

values, it shows that the yield index is maximum at frequencies higher than 2×10^6 Hz for water and 10^5 Hz for ethanol.

Fig. 6 enables the comparison of yield indices and operating parameters for suspension fluids – water and ethanol – with different properties. In this work, a layer of a photoresist was coated on the electrodes (see section 4.3). To calculate the yield index, the capacitance of the photoresist has to be included while calculating C_{eq} in eqn (8). The resulting yield index with ethanol, plotted in Fig. 6(d), shows that the yield index increases slightly from 0.98 to 0.99, when moving from 10^5 to 2×10^5 Hz. However this frequency change would cause the term $\mathrm{Re}[F_{CM}]$ in the DEP force to decrease in value by nearly an order of magnitude from 6×10^{11} to 9×10^{10} (from the data used to create Fig. 3(a)). In this case, we chose a frequency of 10^5 Hz and gave up the small increase in the value of the yield index available at 2×10^5 Hz, to prevent the large reduction in DEP force.

2.5 Clamping

Field-directed assembly typically requires clamping of the NWs, to secure them in place for a circuit or network (integration), or to build individually addressable NW devices. These may require, at one or both ends of a NW, electrical contact or a firm pedestal for nanomechanical applications of NWs. Here we briefly discuss clamping and the post-clamped device yield. Methods such as electron beam induced deposition (EBID)[18] incur a cost proportional to the number of clamped devices; their cost becomes prohibitive for large arrays. Simultaneous electrodeposition of all required clamps on a chip, using the metal electrodes designed for DEP, circumvents this cost penalty. Electrodeposition of gold from cyanide-based solutions has been demonstrated, in previous work with metal NWs[5] and with silicon NWs,[15] to enable clamps of repeatable rigidity. Here, the use of silver (Ag) in place of gold enables reduction in the step cost (current cost ratio 1 : 65 for Ag : Au) and removes the dependence on toxic gold cyanide solutions. Fig. 7 shows a clamp fabricated to create a cantilevered NW with (inset showing) uniform interfacial contact of Ag.

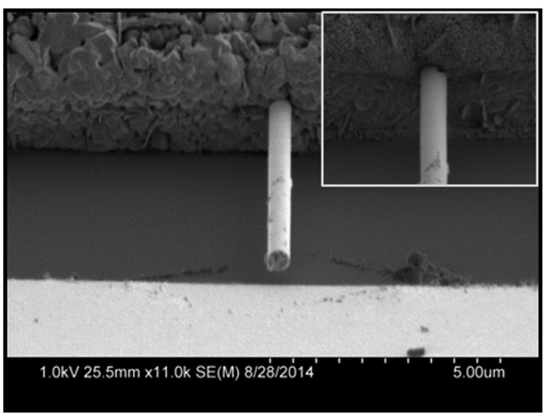

Fig. 7 Single-end-clamped nanoresonator using electrodeposited silver as the clamp material, with the inset showing the uniformity of the silver clamp around the NW.

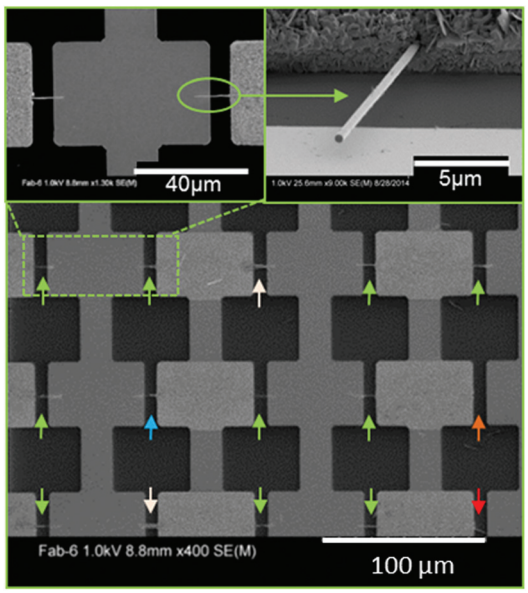

Fig. 8 Array showing well-clamped NWs and examples of defects. Green arrows: perfectly positioned and clamped NWs; blue arrow: a broken NW after clamping and removing the photoresist; white arrow: NW bundle instead of a single NW; orange arrow: no NW; red arrow: misaligned NW.

Fig. 8 is selected to illustrate the examples of defects – empty sites and NWs broken or misaligned during clamping in a high yield post-clamped array. More examples are provided in Fig. S4 and S5.† Other defects such as chained and multiple NWs are rarely seen, following our control of NW concentration. The inset shows a single clamped NW suspended about 500 nm above the electrode surface and free to serve as a mechanical resonator.

Since the post-clamped yield can be lower than the yield from the assembly process alone, for a meaningful comparison of the results of different approaches, it is important to check which one is implied in published reports. For example, the 80% yield quoted in the work of Li *et al.*[15] refers to post-clamped yield and may be compared with the 88% yield in the current study. Freer *et al.*[12] and Collet *et al.*[19] each introduce innovations, with new directors for yield enhancement. Using microfluidic channel flow[12] and capillary force,[19] yields of 98.5% and 81% respectively, were reported by these groups. These studies do not attempt clamping, hence, the numbers from these studies should be compared with the pre-clamped yield of 94% in this work.

2.6 Towards a generalized director–disruptor framework

The entry to the literature on electrohydrodynamic (EHD) field-directed assembly of NWs to date may seem daunting to a new user. This comes from the fact that a number of effects such as DEP, electroosmosis, electrode polarization and electrothermal are involved, with varying roles reported in

Table 2 Table of comparison: identifying director and disruptor forces influencing the yield of single NW assembly in selected studies focused on increasing the yield of individually addressable single NWs. Effects marked by ‡ are classified as director or disruptor by us, based on qualitative information provided in the source. pDEP and nDEP refer to positive and negative dielectrophoreses

Source	Director	Disruptor	Method
This work	• pDEP • Capillary inside wells	• nDEP • High NW concentration • Capillary at drying front • Electroosmosis • Electrode polarization newline • Low pDEP at very high frequency • Electrothermal fluid flow	Analytical & experimental
Collet *et al.*[19]	• pDEP • Capillary	• Very high pDEP • Electrode polarization‡	Analytical & experimental
Palapati *et al.*[18]	• Low DEP force at pDEP to nDEP transition frequency	• Electrode polarization	Computational & experimental
Freer *et al.*[12]	• Hydrodynamic drag force in microfluidic channels • pDEP • Electrostatic repulsion between NW–NW and NW-electrode	• Very high pDEP • Hydrodynamic drag force in microfluidic channels	Analytical & experimental
Burg *et al.*[20]	• pDEP	• Electrothermal fluid flow • Electroosmosis	Computational & experimental
Raychaudhuri *et al.*[14]	• pDEP	• Electroosmosis • Electrode polarization • Low pDEP at very high frequency	Analytical & experimental
Li *et al.*[15]	• pDEP • Capillary inside wells	• Electrode polarization‡ • Capillary in drying front‡	Analytical & experimental
Smith *et al.*[13]	• pDEP	• Very high pDEP • Electrode polarization‡	Analytical & experimental

different studies. A few examples listed in Table 2, show that the same effect can serve either as a director or a disruptor. For example, the capillary force at the moving front is a disruptor in this work and a director in ref. 19; positive DEP (pDEP), the main director for all studies, can be a disruptor at high magnitudes[9,12,19] as it can cause the NW to attach on the electrodes instead of in the gap between them[19] or lead to positioning more than one NW between the electrodes;[9,12] low pDEP is identified as a director in ref. 18 and a disruptor in ref. 14 and in our study. The intensity of each effect as well as its degree of coupling with others, varies in these studies. Further, each one of several physical parameters such as geometry, material properties and frequency, and the magnitude of the applied voltage, can contribute to more than one effect.

The focus of this study is the introduction of a general framework for field-directed NW assembly processes, not limited to DEP, which will help to choose parameter values to maximize the device yield. For any field-directed assembly process we propose a systematic procedure with the steps listed below. The sections of this paper where the work done serves as an example for each step, are noted in brackets below:

1. List the relevant effects and identify the physical parameters involved for each one. See {sections 2.1 and 2.2}.

2. Identify each effect as a possible director or disruptor {sections 2.1 and 2.2}.

3. Where possible, estimate which disruptors are too weak to be significant; discard them {sections 2.1.4 and 2.1.5}.

4. Identify disruptors that are not strongly coupled with any director – remove them, wherever possible, by experimental modification {sections 2.1.1, 2.1.2 and 2.1.3}.

5. Examine the remaining effects for which director–disruptor coupling could be strong-typically where both are either increased or decreased by the same change in any single physical parameter {section 2.2}.

6. Use physical intuition, experiments, analysis or computation, to seek a minimal set of the simplest non-dimensional parameters that represent the competition between the remaining directors and disruptors well enough to be the indicators of yield {section 2.4}.

For the example protocol of DEP discussed in this work, using steps 1 to 6, we found that a single non-dimensional parameter, the yield index, can be used to represent the competition between the director (pDEP) and the strongly-coupled disruptors (electroosmosis and electrode polarization).

The number for the yield index should not be interpreted as the expected value of pre-clamped NW yield – *e.g.* a yield index of 0.94 is not the same as the expectation of the 94% pre-clamped yield. The yield index β which we have defined has the value 1 if the disruptors are negligible and the value 0 if the disruptors dominate and prevent DEP from functioning. The value of β is a guide which tells us how to move in the direction of disruptor reduction. We first determined the frequency (here, 10^5 Hz) to make β close to 1. Further increase in the frequency would yield small disruptor reduction, but it would significantly reduce the DEP force due to the reduction

of Re[F_{CM}] as discussed in section 2.4. Therefore, we fixed the frequency. In order to increase the DEP force to try and achieve the best yield possible, the applied voltage was increased, as shown in Fig. 4.

Apart from the primary use of the yield index discussed above, we note that the framework with the resulting equations, can be useful even after a good working set of parameters for a high yield index is finalized, and a high yield experimentally confirmed. Experimental considerations other than those related to the DEP assembly may impose a new constraint on one of the parameters such as the electrode gap size, or properties of the medium, or the frequency of the field. Considerable effort would be required to arrive at a new set of parameter values by experimental trial-and-error alone. Following the steps of the framework and equations given in sections 2.1, 2.2 and 2.4, one can quickly obtain the working estimates for the remaining parameters, and use them to guide experiments confirming the best values.

This approach enabled a selection of physical parameters to significantly improve the post-clamped yield with respect to the earlier study of Li *et al.*[15] and obtain a pre-clamped yield value close to the maximum yield reported to date by Freer *et al.*,[12] but without the additional experimental cost and complexity of implementing microfluidic channels.

3 Conclusions and outlook

Field-directed assembly enables large-area coverage with individually addressable NW devices. The assembly cost is independent of the area, with potential to aid nanoscale research and to open a path for nanomanufacturing. This study introduces a general director–disruptor framework of steps applicable to any field-directed NW assembly process.

One of several directed assembly methods from the literature with positive dielectrophoresis as the main director was selected to serve as an example, to test the utility of the framework. We identified potential disruptors and estimated those that were weak, or weakly-coupled with the director. With guidance from analysis, computation, or experiment in this and earlier published work, we eliminated weak disruptors and defined constraints between variables for the weakly coupled disruptors. We then proposed a definition for a non-dimensional yield index, to capture the competition between the remaining disruptors and directors. The identification of constraints, as well as the definition of appropriate dimensionless parameters, improves intuition in the assembly process, reduces the dimension of the parameter space and enables the determination of parameter values with far less trial-and-error. The values of several experimental parameters, such as the electrode area and gap size, properties of the suspension medium and frequency of the applied field, were reflected in the yield index. Guided by the variation of the yield index, we obtained the maximum yield (88%) of functional (post-clamped) devices among published reports we have found in the literature to date.

The constraints and dimensionless parameters (such as the yield index here) should be determined afresh for any new field-directed assembly method. Once determined, they provide a rational path for selecting new parameter values, with greatly reduced trial-and-error, if any experimental parameter needs to be changed for reasons other than assembly process. In doing so, the director–disruptor framework enables a better understanding of each field-directed assembly process. It provides a path towards manufacturing large arrays of NW devices at reasonable cost. This is crucial for making use of the commercial and scientific potential of the extraordinary capabilities of NW devices.

4 Experimental methods

4.1 Nanowire synthesis

Rh NWs were synthesized in porous membranes from an aqueous rhodium sulfate solution (RH221D from Technic). NWs with a length up to 12 μm were synthesized by electrodeposition at −400 mV with respect to a Ag/AgCl reference electrode in 60 minutes.[32] Nanoporous AAO membranes with 200 nm nominal pore size and a thickness of 60 μm (Whatman) and polycarbonate membranes with 400 nm nominal pore size and a thickness of 20 μm (Sterlitech) were used for NW synthesis. NWs extracted from the polycarbonate template are closer to a perfect cylinder than NWs synthesized in AAO templates. If this is important, the use of a polycarbonate template is recommended. After dissolving the template (AAO by 3 M NaOH and polycarbonate by dichloromethane), the NWs were suspended in ethanol. Electrodeposition experiments were controlled using a Princeton Applied Research VersaStat3 potentiostat/galvanostat. A detailed discussion of the NW synthesis is available in earlier work.[32]

4.2 Nanowire concentration measurement

A known volume of the NW suspension was dried on a silicon substrate. Fifty non-overlapping optical micrographs, including the center and edge regions of the dried-out drop were analyzed using ImageJ software and the average NW count was used to compute the total number of NWs in the sample. We found that concentrations above 3.3×10^8 NW per mL result in widespread multiple layers or clumps of NWs on the substrate which do not allow a credible count of NWs with this method. For assembly, we found that a concentration two orders of magnitude below this value was required to prevent chaining and multiple NWs per die.

4.3 Nanowire assembly

Six separate dies, each with 9500 NW assembly sites defined by electrode pairs with different gap sizes, were patterned using photolithography and metal lift-off on a silicon substrate with 300 nm of wet thermal oxide. Fig. 1 illustrates the patterning steps to which the following details apply: (a) patterning a ~1 μm thick layer of a deep ultraviolet (DUV) PMGI SF-11 photoresist (MicroChem) hard-baked (at 200 °C for 5 min) to

create wells for trapping NWs between each electrode pair. The wells are ~500 nm deep with lengths of 12, 14 and 16 μm for the electrode gap sizes of 6, 8 and 10 μm respectively (b) micro-pipetting 10 μL of the suspension over each die, with an AC voltage applied across all chosen electrode pairs to trap NWs within the wells. A layer of the Shipley 1811 photoresist (MicroChem), ~1 μm thick was then spun and patterned to create a photoresist mask for exposing the PMGI layer over one electrode of each pair, to enable clamping of the NW end (c) electrodeposition of Ag, from the Silver Cyless (succinimide) solution (Technic), to clamp one end of the NWs, followed by (d) removal of all photoresist and critical point drying.

The PMGI photoresist was chosen in this process for several reasons. Ethanol dissolves Novolac-based photoresists such as Shipley 1811, but it does not dissolve the hard-baked PMGI photoresist. Therefore, the electric-field assisted NW assembly, using NWs suspended in ethanol, was conducted on hard-baked PMGI as an insulating layer to prevent short circuit occurrence for the large-scale NW assembly. Finally, Shipley 1811 and hard-baked PMGI can be exposed at different wavelengths, enabling patterning of PMGI using DUV flood exposure through the Shipley mask.

The chief advantages of this fabrication sequence are: {a} capture of NWs at predetermined well locations, {b} retention of NWs by the capillary force at the surface of the evaporating medium inside the wells and {c} removal of randomly scattered NWs with the photoresist in the last step. This fabrication method eliminates the disruptive effect of a high value of the dielectrophoretic (DEP) force, reported by Collet *et al.*,[19] which causes undesirable NW attachment at several points on the electrodes.

The dielectrophoretic assembly process was performed using a Signatone 1160 probe station. A function generator (Tektronix CFG253) was used to apply frequencies up to 100 kHz and voltages up to 7 V (rms). A Canon 60D digital camera was used to observe the assembly of NWs. The post-clamped NWs were studied using Field Emission Scanning Electron Microscopy (FESEM, Hitachi S-4800).

4.4 Nanowire yield measurement

The percentage yield was computed from 500 out of 9500 randomly selected wells per die (3000 of 57 000 wells per wafer). Optical micrographs provided in the ESI (Fig. S2–S5†) show blank sites and other defects observed during the counting process. For measuring the pre- and post-clamped yield, if multiple NWs were positioned between electrodes, only one NW per electrode pair was counted. Also, when a positioned NW bridged less than half the gap-width as shown in Fig. S4,† it was not counted.

Appendix

Scaling analysis – Brownian and dielectrophoretic displacement

Under the action of the viscous drag force (F_d), given in eqn (14), the terminal velocity u is achieved when viscous drag force F_d opposing the motion becomes equal to the applied DEP force F_{DEP}.

$$F_d = 4u\pi\eta L/[\ln(2L/d) + 0.5] \quad (14)$$

For a NW of mass m, the acceleration changes from $a = (F_{DEP}/m)_{start}$ to zero, as the velocity increases from zero to u, at which time, $F_d = (F_{DEP})_{start}$. For a rough estimate of the time scale,

$$\tau \cong \frac{u}{a} = \frac{\rho_p d^2}{16\eta}[\ln(2L/d) + 0.5] \quad (15)$$

For a rhodium NW with the density ρ_p = 12 410 kg m^{-3}, L = 10 μm, d = 0.25 μm and ethanol dynamic viscosity η = 1.2 × 10^{-3} kg m^{-1} s^{-1}, we calculated τ to be 1.2 × 10^{-7} s. Comparing this time to the observation time t ~1 s, the moving NW is almost always at the terminal velocity. Using the relationship for Brownian displacement with the Stokes–Einstein relationship for particle diffusivity yields[22] $\Delta X_{Br} = (2k_BTt/\gamma)^{1/2}$. The displacement due to the DEP force is $\Delta X_{DEP} = ut = (F/\gamma)t$. The ratio of displacements, used in the order of magnitude analysis in section 2.1.4, is then given by:

$$\Delta X_{Br}/\Delta X_{DEP} = \sqrt{(2K_BT)/(u^2\gamma t)} = \sqrt{(2K_BT\gamma)/(F^2 t)} \quad (16)$$

Acknowledgements

This work was supported by grants from the Natural Sciences and Engineering Research Council of Canada (NSERC) Discovery and RTI programs, as well as from the Canada Foundation for Innovation (CFI) and the British Columbia Knowledge Development Fund (BCKDF). It made use of the 4D LABS shared facilities supported by CFI, BCKDF, as well as Western Economic Diversification Canada (WD), and Simon Fraser University (SFU).

References

1 J. Chaste, A. Eichler, J. Moser, G. Ceballos, R. Rurali and A. Bachtold, *Nat. Nanotechnol.*, 2012, **7**, 301–304.
2 E. Sage, A. Brenac, T. Alava, R. Morel, C. Dupré, M. S. Hanay, M. L. Roukes, L. Duraffourg, C. Masselon and S. Hentz, *Nat. Commun.*, 2015, **6**, 6482–6487.
3 B. Ilic, Y. Yang, K. Aubin, R. Reichenbach, S. Krylov and H. Craighead, *Nano Lett.*, 2005, **5**, 925–929.
4 A. Heidelberg, L. T. Ngo, B. Wu, M. A. Phillips, S. Sharma, T. I. Kamins, J. E. Sader and J. J. Boland, *Nano Lett.*, 2006, **6**, 1101–1106.
5 M. Li, T. S. Mayer, J. A. Sioss, C. D. Keating and R. B. Bhiladvala, *Nano Lett.*, 2007, **7**, 3281–3284.
6 X. Wu, J. S. Kulkarni, G. Collins, N. Petkov, D. Almécija, J. J. Boland, D. Erts and J. D. Holmes, *Chem. Mater.*, 2008, **20**, 5954–5967.

7 R. B. Bhiladvala and Z. J. Wang, *Phys. Rev. E: Stat. Phys., Plasmas, Fluids, Relat. Interdiscip. Top.*, 2004, **69**, 036307–036305.

8 W. Lu and C. M. Lieber, *J. Phys. D: Appl. Phys.*, 2006, **39**, R387–R406.

9 J. Boote and S. Evans, *Nanotechnology*, 2005, **16**, 1500–1505.

10 J. A. Sioss, R. B. Bhiladvala, W. Pan, M. Li, S. Patrick, P. Xin, S. L. Dean, C. D. Keating, T. S. Mayer and G. A. Clawson, *J. Nanomed. Nanotechnol.*, 2012, **8**, 1017–1025.

11 N. P. Dasgupta, J. Sun, C. Liu, S. Brittman, S. C. Andrews, J. Lim, H. Gao, R. Yan and P. Yang, *Adv. Mater.*, 2014, **26**, 2137–2184.

12 E. M. Freer, O. Grachev, X. Duan, S. Martin and D. P. Stumbo, *Nat. Nanotechnol.*, 2010, **5**, 525–530.

13 B. D. Smith, T. S. Mayer and C. D. Keating, *Annu. Rev. Phys. Chem.*, 2012, **63**, 241–263.

14 S. Raychaudhuri, S. A. Dayeh, D. Wang and E. T. Yu, *Nano Lett.*, 2009, **9**, 2260–2266.

15 M. Li, R. B. Bhiladvala, T. J. Morrow, J. A. Sioss, K.-K. Lew, J. M. Redwing, C. D. Keating and T. S. Mayer, *Nat. Nanotechnol.*, 2008, **3**, 88–92.

16 M. C. Wang and B. D. Gates, *Mater. Today*, 2009, **12**, 34–43.

17 D. Whang, S. Jin, Y. Wu and C. M. Lieber, *Nano Lett.*, 2003, **3**, 1255–1259.

18 N. K. Palapati, E. Pomerantseva and A. Subramanian, *Nanoscale*, 2015, **7**, 3109–3116.

19 M. Collet, S. Salomon, N. Y. Klein, F. Seichepine, C. Vieu, L. Nicu and G. Larrieu, *Adv. Mater.*, 2014, **27**, 1268–1273.

20 B. R. Burg, V. Bianco, J. Schneider and D. Poulikakos, *J. Appl. Phys.*, 2010, **107**, 124308–124311.

21 A. Maijenburg, M. Maas, E. Rodijk, W. Ahmed, E. Kooij, E. Carlen, D. Blank and J. Ten Elshof, *J. Colloid Interface Sci.*, 2011, **355**, 486–493.

22 Y. Liu, J.-H. Chung, W. K. Liu and R. S. Ruoff, *J. Phys. Chem. B*, 2006, **110**, 14098–14106.

23 A. Castellanos, A. Ramos, A. Gonzalez, N. G. Green and H. Morgan, *J. Phys. D: Appl. Phys.*, 2003, **36**, 2584–2597.

24 J. Happel and H. Brenner, *Low Reynolds number hydrodynamics: with special applications to particulate media*, Noordhoff International, 1973, vol. 1.

25 J. Luecke and R. L. McCormick, *Energy Fuels*, 2014, **28**, 5222–5228.

26 T. B. Jones, *Electromechanics of particles*, Cambridge University Press, New York, 1995.

27 N. G. Green, A. Ramos, A. Gonzalez, H. Morgan and A. Castellanos, *Phys. Rev. E: Stat. Phys., Plasmas, Fluids, Relat. Interdiscip. Top.*, 2000, **61**, 4011.

28 M. Z. Bazant, *Electrokinetics and electrohydrodynamics in microsystems*, Springer Science, 2011, vol. 530.

29 B. C. Gierhart, D. G. Howitt, S. J. Chen, R. L. Smith and S. D. Collins, *Langmuir*, 2007, **23**, 12450–12456.

30 P. Mirtaheri, S. Grimnes and O. G. Martinsen, *IEEE Trans. Biomed. Eng.*, 2005, **52**, 2093–2099.

31 M. Z. Bazant, K. Thornton and A. Ajdari, *Phys. Rev. E: Stat. Phys., Plasmas, Fluids, Relat. Interdiscip. Top.*, 2004, **70**, 021506–021524.

32 N. Moghimian, M. Sam and R. B. Bhiladvala, *Mater. Lett.*, 2013, **113**, 152–155.